

Electrons and holes in phosphorene

Pengke Li* and Ian Appelbaum

*Department of Physics and Center for Nanophysics and Advanced Materials,
University of Maryland, College Park, MD 20742*

We present a symmetry analysis of electronic bandstructure including spin-orbit interaction close to the insulating gap edge in monolayer black phosphorus (“phosphorene”). Expressions for energy dispersion relation and spin-dependent eigenstates for electrons and holes are found via simplification of a perturbative expansion in wavevector k away from the zone center using elementary group theory. Importantly, we expose the underlying symmetries giving rise to substantial anisotropy in optical absorption, charge and spin transport properties, and reveal the mechanism responsible for valence band distortion and possible lack of a true direct gap.

I. INTRODUCTION

The experimental isolation of atomically thin 2-dimensional layers from van der Waals-bonded 3-dimensional solids has exposed many new opportunities for revealing unconventional electron transport physics. This research area, famously begun with exfoliation of the semimetal graphene from bulk graphite, has now vastly expanded to include work on related group-IV structures (silicene¹, germanene², and stanene³), and on binary semiconductors such as transition-metal dichalcogenides (WS₂⁴, etc.), topological insulators such as Bi₂Se₃⁵, and the group-III-V insulator boron nitride⁶. However, until recently, little has been done to explore the possibility that other forms of elemental compounds beyond group-IV can be exfoliated into few- or single-layer structures like graphite can. Among candidate bulk source materials, orthorhombic black phosphorus (elemental group V) has emerged as a contender.

The classical literature on this substance, reviewed in Ref. 7, is fairly complete at first glance. Single crystals of this ambient-stable allotrope are typically produced using high-pressure Bridgman growth^{8,9} from which atomic structure was first determined via X-ray diffraction more than 50 years ago.^{10,11} Early experimental results on charge transport¹² were complemented by investigations into both electrical and optical properties^{13,14} and compared with theoretical predictions^{15,16}. Unexpected phenomena including superconductivity¹⁷ up to 13 K and evidence of 2D transport¹⁸ motivated a modest resurgence of interest several decades ago.

Following in the footsteps of graphene’s rise in the past decade, more recent experimental work on black phosphorus has focused on field-effect transistor action using thin multi-layered exfoliated flakes as channel conductor.^{19,20} *Single layer* black phosphorus, dubbed “phosphorene”, is of particular interest but has not yet been incorporated into electrical devices. The properties of this 2-dimensional semiconductor have been studied in detail only by using the familiar machinery for bandstructure calculation. Several groups have addressed this problem using different approaches, including the empirical tight-binding^{21,22}, pseudopotential²³, and *ab initio* (Density Functional Theory (DFT))^{24–28} methods, all of

which can be compared to empirical dispersion relations obtained using Angle-Resolved Photo-Emission Spectroscopy from the clean surface.²⁹ Among the intriguing bandstructure features found are p-type semiconducting bandgap in the visible or infrared region and large excitonic binding energy,^{20,30} prominent anisotropy of effective mass and hence carrier mobility,^{25,26} ultraflat valence band dispersion and possible indirect bandgap, strain-induced gap modification,²⁸ high optical efficiency,³¹ etc.

Despite this abundance of bandstructure results in the available literature, several elementary questions remain unanswered, all of which become crucially important once single-layer phosphorene devices are experimentally realized. For example, what is the origin of the large valence-band effective mass anisotropy? What mechanisms determine whether this material has a truly direct bandgap? What are the optical transition selection rules? What are the dominant wavefunction components that dictate spin-dependent properties? etc. The answers to these questions are essential in providing insight for predictions of the properties of electrons and holes affecting charge and spin transport in this material, and are therefore necessary in developing possible device applications.

Various brute-force numerical schemes can churn out the relevant quantities needed to answer the questions above, but they often come at the expense of obscuring the physics at their root, i.e. the fundamental symmetries manifest in the structure of this physical materials system. In the present paper, we exploit the discrete lattice/wavefunction symmetries in phosphorene using the formal results of group theory to directly answer these questions. By first identifying the symmetry properties of wavefunctions at the Brillouin zone center, we simplify $\mathbf{k} \cdot \hat{\mathbf{p}}$ perturbation theory using the method of invariants³² and matrix element theorem to identify terms contributing to the dispersion and spin-dependent eigenstates of all relevant bands at nearby momenta. All the symmetry-protected properties are captured by $\mathbf{k} \cdot \hat{\mathbf{p}}$ parameters that can be easily verified by numerical calculations and empirically determined by further experiments.

The present paper is organized as follows: Section II provides general information on the symmetry of the phosphorene 2D lattice, from which we analyze the symmetries of constituent atomic orbitals and the nearly free

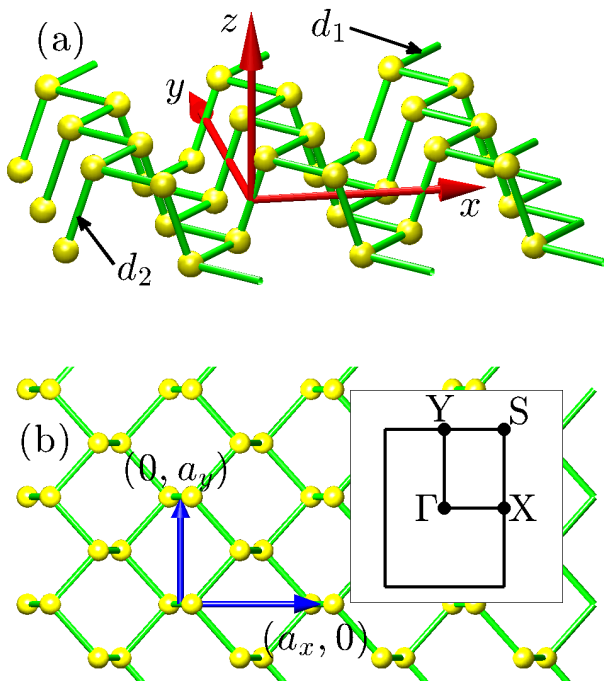


FIG. 1. Orthorhombic lattice of phosphorene. (a) In real-space, two types of bonds between neighboring atoms are indicated by d_1 and d_2 . The origin of the Cartesian coordinates (red arrows) is chosen to be at the center of a d_2 bond. (b) Top view, showing the two lattice vectors (blue arrows). Inset: 2D projection of the reciprocal lattice Brillouin zone, with high symmetry points indicated.

electron model. In Section III, we investigate the spin-independent part of the Hamiltonian using the method of invariants and reveal the fundamental origins of the effective mass anisotropy, especially those interactions resulting in an ultraflat valence band. Optical selection rules are also provided. Using the same approach, in Section IV we focus on the spin-orbit interaction and construct the spin-dependent eigenstates. From these results, we analyze spin relaxation anisotropy before providing a summary and outlook in Section V.

II. SYMMETRY CONSIDERATIONS

A. Lattice symmetry and space group operators

The black phosphorus monolayer is a 2D hexagonal lattice that is buckled, or “puckered”, along the armchair direction. This geometry results in two types of bonds [see Fig. 1(a)]. P atoms connected by bonds parallel to the 2D plane (Type I, with bond length $d_1 = 2.224 \text{ \AA}$) form upper and lower sublayers, while bonds connecting P atoms between these two sublayers (Type II) have a length $d_2 = 2.244 \text{ \AA}$ and are oriented 71.7° out of the plane. In the following discussion, we use Cartesian coordinates with the origin at the center of one Type II

TABLE I. Character table of the Γ -point space group, including basis functions of the IRs. x , y , and z are components of polar vectors, while A_x , A_y and A_z are components of axial vectors.

	E	τC_{2x}	C_{2y}	τC_{2z}	i	τR_x	R_y	τR_z	
Γ_1^+	1	1	1	1	1	1	1	1	
Γ_2^+	1	-1	1	-1	1	-1	1	-1	A_y
Γ_3^+	1	1	-1	-1	1	1	-1	-1	A_x
Γ_4^+	1	-1	-1	1	1	-1	-1	1	A_z
Γ_1^-	1	1	1	1	-1	-1	-1	-1	
Γ_2^-	1	-1	1	-1	-1	1	-1	1	y
Γ_3^-	1	1	-1	-1	-1	-1	1	1	x
Γ_4^-	1	-1	-1	1	-1	1	1	-1	z

bond. The z axis is chosen to be out of plane, with the in-plane x axis along the armchair direction and the y axis transverse to it. In this rectangular $x - y$ basis, the two Bravais lattice constants are $a_x = 4.376 \text{ \AA}$ and $a_y = 3.314 \text{ \AA}$ [see Fig. 1(b)], and within a unit cell there are four P atoms. The inset in Fig. 1(b) shows the first Brillouin zone of this 2D orthorhombic lattice with high symmetry points labeled: Γ -point is the zone center, and X and Y points are at $(\frac{\pi}{a_x}, 0)$ and $(0, \frac{\pi}{a_y})$, respectively, half of the reciprocal lattice vectors.

Phosphorene shares the same in-plane translation symmetry with its bulk counterpart black phosphorus, whose space group is base-centered orthorhombic with international number and symbol $64 : Cmca$.³³ The lattice structure in Fig. 1 provides all necessary information about its nonsymmorphic space group, whose factor group is isomorphic to the point group D_{2h} . There are eight elements in this nontrivial factor group; each of them is a coset about the direct product of a symmetry operator and the lattice vector translation subgroup T . Among these eight symmetry operators, four are pure rotations (either proper or improper), including the identity operator E , the space inversion operator i , the operator corresponding to 180° rotation around the y axis C_{2y} , and the operator corresponding to reflection with respect to the $y = 0$ plane R_y . The remaining four are a translation $\tau = (\frac{a_x}{2}, \frac{a_y}{2})$ in addition to pure rotations, including τC_{2x} , τC_{2z} , τR_x and τR_z . Since the D_{2h} group is abelian (commutative), each group element forms a single class.

The most important information about the symmetry of this space group and its eight irreducible representations (IRs) is included in the character table (see Table I). Since this is the same group as that of the Brillouin zone center Γ -point, these IRs are denoted by $\Gamma_i^{+(-)}$, with subscript $i = 1, 2, 3, 4$, and superscript $+$ ($-$) indicating even (odd) parity under the inversion operator. In this table we also list the basis functions of some IRs. Here, x , y and z are components of a polar vector (e. g. the momentum operator $\hat{\mathbf{p}}$) while A_x , A_y and A_z are those of an axial, or “pseudo-”, vector (essential for analyzing the effect of spin-orbit interaction with vector field $\propto \nabla V \times \hat{\mathbf{p}}$).

In the following subsection, we will briefly discuss the

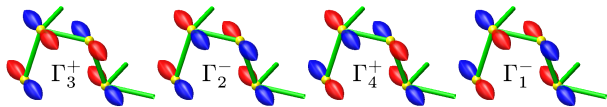


FIG. 2. Four configurations of the p_y orbitals within a unit cell, together with their associated IRs, all of which are odd under the reflection operator R_y . They represent the four zone-center eigenstates composed solely from the pure p_y atomic orbitals. From left to right, the eigenenergies of the four orbital states decrease [$E(\Gamma_3^+) > E(\Gamma_2^-) > E(\Gamma_4^+) > E(\Gamma_1^-)$], according to the bonding or antibonding nature of the covalent bonds between neighboring atoms. Note that the Γ_2^- configuration also represents the long-wavelength acoustic phonon mode where all atoms move in-phase along the zigzag direction.

symmetries of the atomic orbitals and the empty lattice “nearly free” electron band structure at the Γ -point, using the information in Table I. These considerations provide intuition on the symmetry-related coupling of the eigenstates near the zone center and are important for understanding the overall electronic structure.

B. Atomic orbital symmetries at the center of the Brillouin zone

The band structure of black phosphorus was studied by Takao *et. al.*²¹ with a spin-independent tight-binding model using a basis of one s orbital and three p orbitals. With four P atoms within a unit cell, there are therefore sixteen bands. By calculating the hopping energy and orbital overlaps between neighboring atoms, they determined the band gaps of black phosphorus in the form of monolayer and bulk, and indexed the symmetries of eigenstates at the Γ -point. In general, wavefunctions constructed this way will consist of sp^3 hybridized atomic orbitals. However, at the zone center, the p_y orbital (which is odd under R_y) is isolated from the remaining s , p_x and p_z orbitals that remain mixed (similar to the case of pure p_z orbitals in monolayer graphene due to the R_z operator).

According to the character table (Table I), all the sixteen eigenstates at the Γ -point are nondegenerate, since all the IRs are one-dimensional. Four of these IRs, associated with the four p_y orbital configurations illustrated in Fig. 2, are odd under the reflection operator R_y : Γ_3^+ , Γ_4^+ , Γ_1^- and Γ_2^- . The bonding energy is dominated by Type I bonds (within each sublayer) that hybridize $pp\pi$ and $pp\sigma$ covalent chemical bonds, the latter of which is much stronger due to higher orbital overlap. Type II bonds (connecting the two sublayers) are pure but weaker $pp\pi$ bonds and have only a secondary contribution to the bonding energy. By considering the bonding and antibonding nature of the p_y orbitals, we give in Fig. 2 the relative order of the four eigenenergies, which matches the tight-binding calculation²¹.

Takao *et. al.* gave the p_z orbital configurations at the

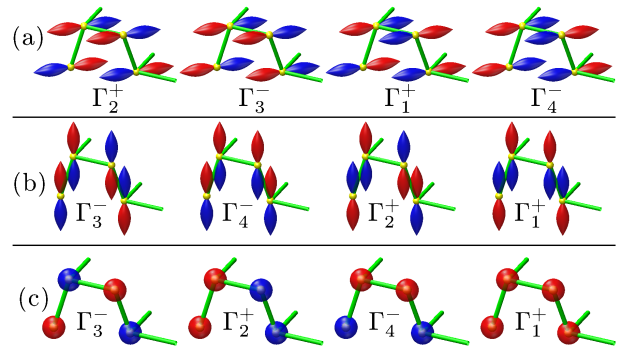


FIG. 3. Same as Fig. 2, here for (a) p_x , (b) p_z and (c) s orbitals that are even under the reflection operator R_y . IRs in each row are listed from left to right in descending order of total covalent bond energy. Similar to Γ_2^- in Fig. 2, here we see configurations corresponding to the remaining two long wavelength acoustic phonon modes: Γ_3^- in (a) corresponds to in-plane motion along the armchair direction while Γ_4^- in (b) corresponds to out-of-plane (flexural) phonons.

bandgap edge (Γ_2^+ for the valence band and Γ_4^- for the conduction band). In Fig. 3(a), (b), and (c), we list the configurations of all the p_x , p_z and s orbitals, respectively, for the four IRs Γ_1^+ , Γ_2^+ , Γ_3^- and Γ_4^- that are even under the reflection operator R_y , and order them according to their bond energy. Within the sp^3 tight-binding model, each of these four representations corresponds to three bands, among which the contributions of p_x , p_z and s orbital components with the same symmetry vary.

Similar to our discussion of the p_y orbital, we now examine the bonding or antibonding characteristics of these atomic orbital configurations and determine the relative energy ordering of the eigenstates. In the following sections we will focus on the band edge states which belong to Γ_2^+ and Γ_4^- , both dominated by the p_z orbital. In this case [see Fig. 3(b)], $pp\sigma$ bonds are within the Type II bonds, which are bonding (antibonding) in Γ_2^+ (Γ_4^-) with lower (higher) energy assigning it the top of the valence band (bottom of the conduction band).

Using the first-principles calculation package QUANTUM ESPRESSO³⁴, we studied this energy order of the Γ -point eigenstates. Different density functionals and pseudopotentials chosen as input to the *ab initio* calculation vary the detailed values of energy differences at the Γ point as well as the dispersion curves away from it. However, the band ordering at the Γ point is consistent with those given by Takao *et. al.* (only a few bands very close in energy switch places). This verifies that the order of the Γ point eigenstates is generally determined by the symmetries of the atomic orbitals alone.

C. Empty-lattice band structure

The atomic orbitals give a perturbative picture of the electronic structure in the tight-binding regime. A useful

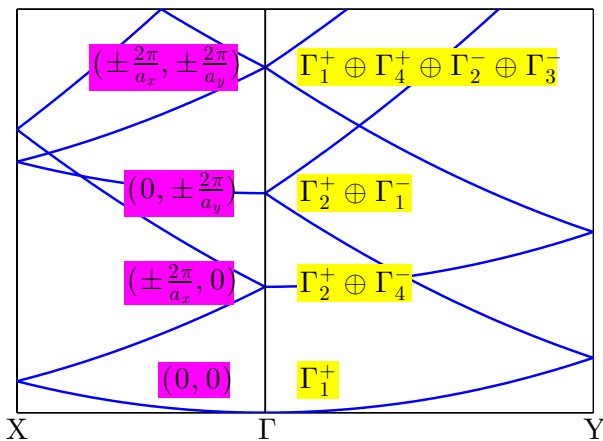


FIG. 4. Free-electron bandstructure, including symmetry labels (yellow) of zone-center eigenstates formed from superpositions of plane-waves centered at the reciprocal lattice points indicated (purple).

approximation in the opposite (delocalized) extreme is the nearly-free electron model that describes the empty-lattice band structure, in which the electronic states are pure plane-waves with wave numbers given by the reciprocal lattice vectors (\mathbf{G}_n). Using projection operators, we obtain the symmetrized wavefunctions which are linear combinations of plane-waves degenerate at the Γ -point. When the atomic potentials are introduced into this nearly free electron model, only those symmetrized wavefunctions belonging to the same IR can be linearly combined to form the real eigenstates (the symmetry of the eigenstates from empty-lattice to the real lattice is maintained) and result in broken degeneracy with the possibility of bandgaps.

An important potential concern with this approach is that it does not account for the transformation properties of the wavefunctions under out-of-plane reflection. Therefore, in principle, wavefunctions constructed in this way provide only incomplete symmetry properties. However, since the dynamical characteristics of interest involve only in-plane symmetries, the simple nearly-free electron model can indeed provide sufficient information.

Because of the orthorhombic symmetry of monolayer black phosphorus, the degeneracy of nearly-free electron states at the Γ -point can only be singlet ($\mathbf{G}_n = 0$), doublet (\mathbf{G}_n on the k_x or k_y axes) or quartet (general \mathbf{G}_n). Fig. 4 shows the empty-lattice band structure including the lowest nine Γ -point eigenstates. In the following sections, we will show that the in-plane momentum matrix elements $\langle \hat{p}_{x,y} \rangle$ of the zone center eigenstates play a fundamental role in determining the electronic structure of phosphorene. The nearly-free electron model explicitly shows that $\langle \hat{p}_{x,y} \rangle$ are nonzero only between degenerate states with relevant wavevector components. For instance, for the doubly degenerate first excited states in the form of symmetrized wavefunctions

with $\mathbf{G}_n = (\pm \frac{2\pi x}{a_x}, 0)$, we have

$$\langle \Gamma_2^+ | \hat{p}_x | \Gamma_4^- \rangle = \langle \cos \frac{2\pi x}{a_x} | \frac{\hbar}{i} \frac{\partial}{\partial x} | \sin \frac{2\pi x}{a_x} \rangle = \frac{2\pi \hbar}{a_x}, \quad (1)$$

while $\langle \Gamma_2^+ | \hat{p}_y | \Gamma_4^- \rangle = 0$. Similarly, \hat{p}_x and \hat{p}_y between either of these two states and any other remaining Γ -point plane-wave state vanish, consistent with the matrix element theorem as discussed below.

III. SPIN-INDEPENDENT PROPERTIES

In this section, we study the spin-independent band structure properties close to the bandgap in phosphorene. We construct the $\mathbf{k} \cdot \hat{\mathbf{p}}$ Hamiltonian near the zone center using the method of invariants,³² and show that the dispersion relation of the conduction band and valence band can be captured by an effective mass approximation only in the k_x direction, while in the k_y direction the unique coupling from remote bands can potentially lead to an indirect bandgap.

A. Hamiltonian and method of invariants

Following conventional $\mathbf{k} \cdot \hat{\mathbf{p}}$ theory, the Hamiltonian is given by

$$H = H_0 + H_{\mathbf{k} \cdot \hat{\mathbf{p}}} + H_{\text{SO}} + H_{\text{SO},\mathbf{k}}, \quad (2)$$

where

$$H_0 = \frac{\hbar^2}{2m_0} (k_x^2 + k_y^2), \quad (3)$$

$$H_{\mathbf{k} \cdot \hat{\mathbf{p}}} = \frac{\hbar}{m_0} (k_x \hat{p}_x + k_y \hat{p}_y), \quad (4)$$

$$H_{\text{SO}} = \frac{\hbar}{4m_0^2 c^2} \nabla V \times \hat{\mathbf{p}} \cdot \vec{\sigma}, \quad \text{and} \quad (5)$$

$$H_{\text{SO},\mathbf{k}} = \frac{\hbar^2}{4m_0^2 c^2} \left[(k_x \sigma_y - k_y \sigma_x) \frac{\partial V}{\partial z} + k_y \sigma_z \frac{\partial V}{\partial x} - k_x \sigma_z \frac{\partial V}{\partial y} \right]. \quad (6)$$

Here, H_0 is the in-plane free electron dispersion, and $H_{\mathbf{k} \cdot \hat{\mathbf{p}}}$ is the $\mathbf{k} \cdot \hat{\mathbf{p}}$ term to be treated perturbatively. In this section we will focus on these two spin-independent terms. The spin-related properties are captured by the \mathbf{k} -independent H_{SO} and \mathbf{k} -dependent $H_{\text{SO},\mathbf{k}}$ terms, and are discussed in the subsequent section. Note that for light atoms like phosphorus, the interaction strength hierarchy is generally $H_{\mathbf{k} \cdot \hat{\mathbf{p}}} \gg H_{\text{SO}} \gg H_{\text{SO},\mathbf{k}}$.

Given the symmetry of the problem, we naturally choose to represent this Hamiltonian in a basis defined by the spin-independent Γ -point eigenstates. Matrix elements of perturbative terms in Eq. (2) can then be determined by the method of invariants³²: only if the IR associated with the invariant component operator is included

TABLE II. Table of invariants

IRs	Γ_1^+	Γ_2^+	Γ_3^+	Γ_4^+	Γ_2^-	Γ_3^-	Γ_4^-
Invariants	$k_x^2 + k_y^2$	σ_y	σ_x	σ_z	$k_y,$ $-k_x\sigma_z$	$k_x,$ $k_y\sigma_z$	$k_x\sigma_y - k_y\sigma_x$

TABLE III. Direct product between Γ_2^+ (Γ_4^-) and all IRs.

	Γ_1^+	Γ_2^+	Γ_3^+	Γ_4^+	Γ_1^-	Γ_2^-	Γ_3^-	Γ_4^-
Γ_2^+	Γ_2^+	Γ_1^+	Γ_4^+	Γ_3^+	Γ_2^-	Γ_1^-	Γ_4^-	Γ_3^-
Γ_4^-	Γ_4^-	Γ_3^-	Γ_2^-	Γ_1^-	Γ_4^+	Γ_3^+	Γ_2^+	Γ_1^+

in the direct sum decomposition of the direct product of the two IRs of the basis functions can the matrix element be nonzero. In Table II, we list the association of the IRs with all the invariant components of terms in Eq. (2) according to their transformation properties under the symmetry operators in Table I.

Our main focus is on the lowest conduction band and the highest valence band, which belong to the IRs Γ_4^- and Γ_2^+ , respectively. For convenience, we list the direct product of these two IRs with all IRs in Table III. In particular, we will reveal the origin of the anisotropy of the energy dispersion relation in the k_x and k_y directions, which is naturally endowed by the orthorhombic symmetry of the crystal lattice.

B. Effective mass of electrons and holes in the k_x direction

With the help of Table II, we see that the perturbative term proportional to $k_x\hat{p}_x$ in Eq. (4) belongs to Γ_3^- . This term directly couples the lowest conduction band and the highest valence band in off-diagonal matrix elements ($\Gamma_3^- = \Gamma_4^- \otimes \Gamma_2^+$; see Table III). Similarly, the term proportional to k_x^2 in Eq. (3) belongs to Γ_1^+ and corresponds to diagonal matrix elements $\Gamma_4^- \otimes \Gamma_4^-$ and $\Gamma_2^+ \otimes \Gamma_2^+$. Notice that the second lowest conduction band also belongs to Γ_2^+ and therefore is expected to affect the Γ_4^- bottom conduction band significantly as well. Given the fact that all other remote bands belonging to Γ_2^+ or Γ_4^- are much further away in energy, we can describe the k_x direction dispersion relation close to the bandgap by a minimal 3×3 Hamiltonian with a basis of $\{\Gamma_{2c}^+, \Gamma_{4c}^-, \Gamma_{2v}^+\}$ (where the subscripts v and c indicate ‘valence’ and ‘conduction’, respectively):

$$H_{3 \times 3} = \begin{pmatrix} E_1 + E_g + \frac{\hbar^2 k_x^2}{2m_0} & P_{x2}k_x & 0 \\ P_{x2}k_x & E_g + \frac{\hbar^2 k_x^2}{2m_0} & P_{x1}k_x \\ 0 & P_{x1}k_x & \frac{\hbar^2 k_x^2}{2m_0} \end{pmatrix}, \quad (7)$$

where E_g is the bandgap at the Γ -point, E_1 is the energy difference between Γ_{2c}^+ , and Γ_{4c}^- , and the off-diagonal ma-

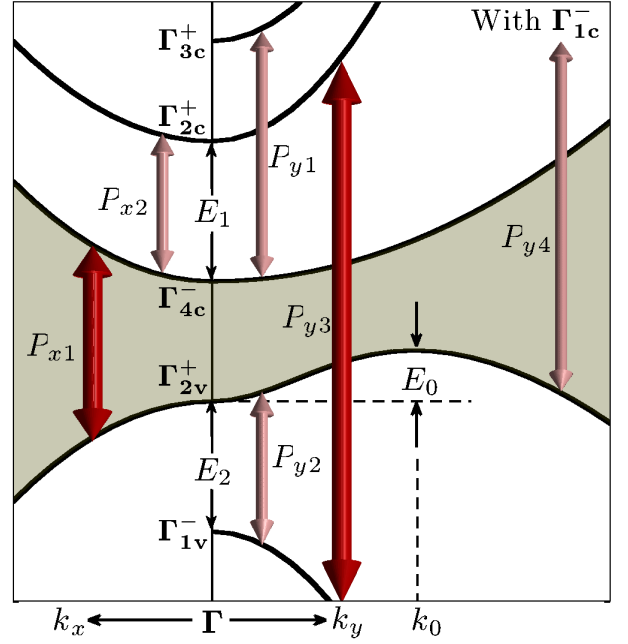


FIG. 5. Schematic bandstructure of phosphorene near the zone center, illustrating the relevant perturbative interactions allowed by symmetry. Red double arrows indicate dominant coupling terms, and pink arrows highlight important non-negligible additional interactions. The gray region represents the forbidden gap. See Eq. (19) and related text for conditions resulting in indirect gap ($E_0, k_0 \neq 0$). The plotting of bands are not to scale, especially E_0 is exaggerated for better illustration.

trix elements are dependent on

$$P_{x1} = \frac{\hbar}{m_0} \langle \Gamma_{4c}^- | \hat{p}_x | \Gamma_{2v}^+ \rangle, \quad \text{and} \quad (8)$$

$$P_{x2} = \frac{\hbar}{m_0} \langle \Gamma_{4c}^- | \hat{p}_x | \Gamma_{2c}^+ \rangle. \quad (9)$$

Such couplings are shown by double arrows in Fig. 5 on the k_x side of the Γ -point in a schematic bandstructure. Note that, for zone center wavefunctions, we can always adjust their overall phases so that P_{x1} and P_{x2} are real numbers.

Applying the Löwdin partitioning method³⁵ to lowest order, Eq. (7) yields analytic expressions for the dispersion relations of electrons and holes in the k_x direction:

$$E_e(k_x) = E_g + \frac{\hbar^2}{2m_0} k_x^2 - \frac{P_{x2}^2}{E_1} k_x^2 + \frac{P_{x1}^2}{E_g} k_x^2, \quad \text{and} \quad (10)$$

$$E_h(k_x) = \frac{\hbar^2}{2m_0} k_x^2 - \frac{P_{x1}^2}{E_g} k_x^2. \quad (11)$$

From these eigenenergies, we can then calculate the ef-

fective masses via $\left[\frac{1}{\hbar^2} \frac{d^2 E}{dk_x^2}\right]^{-1}$:

$$\frac{1}{m_{e,x}} = \frac{1}{m_0} - \frac{2P_{x2}^2}{E_1} + \frac{2P_{x1}^2}{E_g}, \text{ and} \quad (12)$$

$$\frac{1}{m_{h,x}} = -\frac{1}{m_0} + \frac{2P_{x1}^2}{E_g}. \quad (13)$$

To evaluate m_e and m_h , we utilize the results of the free electron model in Sec. II C. Our DFT calculations show that both Γ_{4c}^- and Γ_{2v}^+ have a dominant first excited state plane-wave component with $\mathbf{G} = (\frac{2\pi}{a_x}, 0)$, while for Γ_{2c}^+ this component is small and the majority is the second excited state with $\mathbf{G} = (0, \frac{2\pi}{a_y})$, regardless of the DFT details. Thus, the magnitudes of both $m_{e,x}$ and $m_{h,x}$ are largely dictated by the term related to P_{x1} [illustrated in Fig. (5) by the large red double arrow on the k_x side], with amplitude on the order of $\frac{2\pi\hbar^2}{m_0 a_x}$ [see Eq. (1)], while the P_{x2} -related term is a small correction to $m_{e,x}$ that reduces the difference between $m_{e,x}^{-1}$ and $m_{h,x}^{-1}$.

It should be noted that a recently-proposed two-band model yields a similar dispersion relation in the k_x direction.²⁸ In that model, it is claimed that the effect of the Γ_{2c}^+ conduction band (as well as the contribution of remote bands) has been lumped into off-diagonal matrix elements by terms quadratic in k after Löwdin partitioning. We are compelled to point out that this result is flawed, however, since k_x^2 is not an invariant of $\Gamma_4^- \otimes \Gamma_2^+ = \Gamma_3^-$, and Löwdin partitioning always maintains the underlying symmetry. Furthermore, inclusion of specious odd-power terms in the eigenenergies (due to the coupling of the off-diagonal linear and quadratic terms) breaks time-reversal symmetry such that dispersions in $+k_x$ and $-k_x$ directions are unphysically different. For the same reason, the off-diagonal k_y^2 term in that two-band model (leading to a k_y^4 dispersion relation) is also incorrect. In the following subsection, we will show the correct origins of the flat valence band and possible indirect bandgap in the k_y direction.

C. Dispersion relation in the k_y direction

Unlike the case in the k_x direction, direct coupling of the band edge states Γ_{2v}^+ and Γ_{4c}^- is absent in the k_y direction; energetically-remote bands must therefore be taken into account. The situation for the conduction band is relatively simple: according to Tables II and III, the invariant component k_y belongs to Γ_2^- and couples Γ_{4c}^- to Γ_3^+ states. As discussed in Sec. II B, within the sp^3 tight-binding model giving the lowest sixteen bands, Γ_3^+ is the highest energy state among the four pure p_y orbitals. Numerical calculation shows that it lies beyond Γ_{4c}^- ,²¹ consistent with our DFT calculation. Together with other (even higher) states with the same symmetry, Γ_{3c}^+ repels the dispersion of the lowest conduction band downward

via the matrix element

$$P_{y1} = \frac{\hbar}{m_0} \langle \Gamma_{3c}^+ | \hat{p}_y | \Gamma_{4c}^- \rangle. \quad (14)$$

This interaction is schematically shown with a double-sided pink arrow in Fig. 5. Since the plane-wave component of $\mathbf{G} = (0, \frac{2\pi}{a_y})$ in Γ_{4c}^- is relatively small, P_{y1} is not large enough to reverse the conduction band's positive curvature. However, it does result in a value of the effective mass larger than m_0 .

The valence band state Γ_{2v}^+ requires a different analysis. According to Table III, and reflected in Fig. 5, Γ_{1v}^- can directly couple to Γ_{2v}^+ via $k_y \hat{p}_y$ perturbation. This state, the lowest among the four pure p_y orbital states (see Fig. 2), compels us to consider a matrix element

$$P_{y2} = \frac{\hbar}{m_0} \langle \Gamma_{1v}^- | \hat{p}_y | \Gamma_{2v}^+ \rangle. \quad (15)$$

Compared with P_{x1} , this quantity is relatively small due to the minority $(0, \frac{2\pi}{a_y})$ plane-wave component in Γ_{2v}^+ (despite its dominant role in Γ_{1v}^-). However, without a counterbalancing interaction, its presence would repel the Γ_{2v}^+ band upward, leading to an electron-like positive effective mass and close the bandgap.

Previous DFT calculation by others has already shown that monolayer black phosphorus potentially possesses an indirect bandgap, in which the maximum of the valence band is located along the k_y direction away from the zone center.²⁸ Using various input density functionals and pseudopotentials, we have verified the persistence of this feature which leads to a small positive energy difference ($E_0 \sim \text{meV}$, depending on the details of the numerical procedures) between the valence band maximum at wavevector k_0 ($\approx 10\%$ from BZ edge) and eigenenergy at the zone center. In contrast to an ordinary quadratic dispersion relation, understanding such unusual band structure requires careful examination of the couplings between Γ_{2v}^+ , Γ_{1v}^- , Γ_{2c}^+ , and further upper conduction bands of Γ_1^- symmetry.

We have mentioned that for both Γ_{1v}^- and Γ_{2c}^+ states, plane-wave component $(0, \frac{2\pi}{a_y})$ dominates the wavefunctions. As indicated in Fig. 5 by a large red double arrow, the direct coupling of these two states by $k_y \hat{p}_y$ in

$$P_{y3} = \frac{\hbar}{m_0} \langle \Gamma_{1v}^- | \hat{p}_y | \Gamma_{2c}^+ \rangle \sim \frac{2\pi\hbar^2}{m_0 a_y} \quad (16)$$

is very large. Thus, the Γ_{1v}^- band is strongly repelled downward along the k_y direction, giving a dispersion

$$E_{1v}(k_y) \approx -E_2 - \frac{P_{y3}^2}{E_1 + E_g + E_2} k_y^2, \quad (17)$$

where E_2 is the energy difference from Γ_{2v}^+ to Γ_{1v}^- . Both the free electron dispersion and the effect from Γ_{2v}^+ [Eq. (15)] are neglected in this expression, due to their minor contributions compared with the influence

of P_{y3} . As k_y increases, the energy difference between Γ_{2v}^+ and Γ_{1v}^- therefore quickly grows, further diminishing their coupling.

An additional interaction is still needed to induce a hole-like negative effective mass for Γ_{2v}^+ to preserve the open bandgap. This role is played by conduction band states with Γ_1^- symmetry, as shown in Fig. 5 by the matrix element

$$P_{y4} = \frac{\hbar}{m_0} \langle \Gamma_{1c}^- | \hat{p}_y | \Gamma_{2v}^+ \rangle. \quad (18)$$

Under the basis functions of $\{\Gamma_{1c}^-, \Gamma_{2c}^+, \Gamma_{2v}^+, \Gamma_{1v}^-\}$, one could construct a 4×4 Hamiltonian similar to Eq. (7), including all important $k_y \hat{p}_y$ interactions affecting the valence band. However, just from the Hamiltonian matrix element analysis in Eqs. (15)-(18), the application of Löwdin partitioning already gives the unusual valence band dispersion in the k_y direction approximated by

$$E_h(k_y) = \frac{\hbar^2}{2m_0} k_y^2 - \frac{P_{y4}^2}{E_3} k_y^2 - \frac{P_{y2}^2 k_y^2}{E_{1v}(k_y)}, \quad (19)$$

where E_3 is the energy difference from Γ_{1c}^- to Γ_{2v}^+ . Note that, in the denominator of the last term, we use the complete dispersion of the Γ_{1v}^- band [Eq. (17)] which is negative and depends on k_y , rather than $-E_2$, the fixed energy difference between Γ_{1v}^- and Γ_{2v}^+ .

Eq. (19) guarantees a hole-like dispersion if the second term (repulsion from Γ_{1c}^-) overcomes the first (free electron) term. The ultraflat valence band along k_y is thus due to the counteracting effects of Γ_{1v}^- and Γ_{1c}^- close to the zone center; phosphorene is indirect-gap ($k_0 \neq 0$) when the matrix element magnitudes satisfy $\frac{P_{y2}^2}{E_2} + \frac{\hbar^2}{2m_0} > \frac{P_{y4}^2}{E_3} > \frac{\hbar^2}{2m_0}$. Although this condition is predicted by DFT, other indications of inaccuracies or variations in that numerical method (for example, gross underestimation of the bandgap or the details of relaxed structure)³⁶ suggest that we cannot exclude the possibility that repulsion from Γ_{1c}^- is so strong that $\frac{P_{y4}^2}{E_3} > \frac{P_{y2}^2}{E_2} + \frac{\hbar^2}{2m_0}$, resulting in a direct gap. The true nature of the valence band must therefore be revealed by experiment.

D. Optical selection rules

The interaction between matter and radiation $\frac{e}{m} \mathbf{A} \cdot \hat{\mathbf{p}}$ has the same symmetry as $H_{\mathbf{k} \cdot \hat{\mathbf{p}}}$ (the electric field of light transforms like an ordinary polar vector). Therefore, we can use the perturbative coupling superimposed as arrows on Fig. 5 to reveal the selection rules of optical transitions between conduction and valence bands in phosphorene.

The dominant transition paths are represented by the two red double arrows. When the electric field polarization is parallel to the x -direction, photons with $\hbar\omega \geq E_g$ can cause excitation across the bandgap from Γ_{2v}^+ to

Γ_{4c}^- . On the other hand, photons with orthogonal polarization parallel to the y -direction can excite lower valence band Γ_{1v}^- electrons to the upper conduction band Γ_{2c}^+ , which requires a frequency deep into the ultraviolet regime ($E_g + E_1 + E_2 \sim 5$ eV photon energy). In addition to the bands shown in Fig. (5) that are relevant to the bandedge dispersion, we note that there are also a Γ_{4v}^+ band between Γ_{2v}^+ and Γ_{1v}^- , as well as a Γ_{3c}^- band in between Γ_{2c}^+ and Γ_{3c}^+ . Optical transition with y -polarization is also allowed between these two states ($\Gamma_{4v}^+ \otimes \Gamma_{3c}^- = \Gamma_2^-$), which are separated by ~ 5 eV but extend along the $\Gamma - X$ axis and reach a minimum energy separation at the location of a valence band satellite valley. This could explain the ~ 3.7 eV onset photon energy in the calculated absorption spectrum of y -polarized light.³⁰

The sensitivity of the absorption spectrum to electric field orientation, confirmed by DFT calculation,²⁶ may make phosphorene an ideal photoconductive polarimeter in near-infrared frequencies.

In anticipation of the next section where we consider spin properties, it is appropriate to point out in the present discussion of radiative selection rules that optical orientation in phosphorene is hopelessly inefficient: Unlike in bulk semiconductors with cubic symmetry, where degeneracy of the p -like valence band is preserved in the spin-independent Hamiltonian allowing strong mixing of spin and orbital angular momentum, here with inversion-symmetric but orthorhombic phosphorene we have only nondegenerate and energetically well-separated bands. Spin-orbit interaction can thus only have a small perturbative mixing of spin states. Illumination with linear polarization almost entirely preserves spin during absorptive transitions, so that excitation of the spin-unpolarized valence band will result only in population of a nearly spin-unpolarized conduction band.

IV. SPIN-DEPENDENT PROPERTIES

The spin-orbit interaction (SOI) in semiconductors composed of light atoms is expected to be weak, resulting in relatively pure spin states and long spin lifetime in the intrinsic regime. By this reasoning, SOI in phosphorus allotropes should resemble that of its neighbor on the periodic table, silicon, an indirect-gap group-IV bulk semiconductor that has a long spin lifetime for electrons in the conduction band³⁷⁻³⁹ and a small split-off energy (44 meV) in the valence band. The latter feature of the bandstructure is a result of the SOI perturbing an otherwise three-fold degenerate p -like valence band extremum. Phosphorene, on the other hand, has only non-degenerate and energy-isolated bands (other than the few accidental crossings). When SOI is included in the calculation, we therefore expect only that some of the bands will be unnoticeably shifted, as confirmed by DFT calculation.²⁶

Although SOI has a negligible effect on the band structure (Hamiltonian eigenvalues) in phosphorene, it is still

worthwhile to examine the effect it has on spin-dependent eigenstates, especially because the in-plane anisotropy is expected to extend to spin-related phenomena such as relaxation mechanisms. In this section, we will now derive the *spin-dependent* Hamiltonian including H_{SO} and $H_{\text{SO},\mathbf{k}}$, again using the method of invariants, and calculate the spin-dependent eigenstates of electrons and holes that capture the underlying symmetries.

Before starting our discussion, we compare some other spin-related properties between phosphorene and silicon, the latter of which is believed to be a promising material candidate for spintronic devices.⁴⁰ Besides the low atomic number already mentioned, there are two important factors leading to the rather long spin lifetime in Si. One is the centrosymmetric property of the diamond lattice that (along with Kramers' time-reversal symmetry) preserves spin degeneracy, and precludes the Dyakonov-Perel spin relaxation mechanism where momentum scattering causes a fluctuating effective magnetic field driving spin flips.⁴¹ The other is the absence of nuclear spin in the most abundant isotope ^{28}Si , so that there is little hyperfine interaction affecting the electron spin states.

Whereas the high abundance of ^{31}P isotope (with half-integer nuclear spin) makes hyperfine interaction in phosphorene worth considering, it is outside the scope of this paper. However, phosphorene is indeed centrosymmetric (see Table I), and so like Si, Dyakonov-Perel spin relaxation is absent. The dominant spin relaxation mechanism in both materials is then the Elliott and Yafet processes.

Generally speaking, perturbative spin-orbit coupling between different bands causes a mixing of pure Pauli spinors so that the two degenerate spin states within the same i th band can be written as

$$|i\uparrow\rangle = C_i \left(|i\uparrow\rangle + \sum_{j \neq i} a_j |j\uparrow\rangle + b_j |j\downarrow\rangle \right), \quad \text{and} \quad (20)$$

$$|i\downarrow\rangle = C_i \left(|i\downarrow\rangle + \sum_{j \neq i} a_j^* |j\downarrow\rangle - b_j^* |j\uparrow\rangle \right), \quad (21)$$

where C_i is a normalization factor. The dominant orbital component in both $|i\uparrow\rangle$ and $|i\downarrow\rangle$ is $|i\rangle$, whose amplitude is very close to unity. However, the coefficients $|b_j| \leq |a_j| \ll 1$ depending on their perturbation origins. In our following discussion, we ignore the prefactor $C_i \approx 1$, and for clarity, write the spin-dependent eigenstates in the form of 2-row matrices such as

$$|i\uparrow\rangle = \begin{pmatrix} a_1 & a_2 & \dots & 1 & \dots \\ b_1 & b_2 & \dots & 0 & \dots \end{pmatrix}, \quad \text{and} \quad (22)$$

$$|i\downarrow\rangle = \begin{pmatrix} -b_1^* & -b_2^* & \dots & 0 & \dots \\ a_1^* & a_2^* & \dots & 1 & \dots \end{pmatrix}, \quad (23)$$

where quantities in the top (bottom) row indicate coefficients of $|\uparrow\rangle$ ($|\downarrow\rangle$) states, and each column corresponds to a given band.

Spin flips are induced by an interaction $\langle \uparrow | \Xi | \downarrow \rangle$, where Ξ is a scattering potential. The spin-independent part

of this potential, normally leading to momentum scattering, will then couple the same spin components of $|\uparrow\rangle$ and $|\downarrow\rangle$, resulting in the Elliot mechanism⁴², whereas the spin-dependent part of the scatterer will couple opposite spin components and give rise to the Yafet term⁴³. These two quantities coherently interfere to yield the total spin relaxation rate τ_s^{-1} , proportional to the square of the matrix element according to Fermi's golden rule. A major goal of the following subsections is to examine the symmetry of these processes and understand the spin-relaxation anisotropy in terms of the spin-dependent eigenstate components.

A. Hamiltonian and spin-dependent eigenstates

The incorporation of spin-orbit interactions [Eqs. (5) and (6)] within the framework of the method of invariants is as straightforward as our treatment of $H_{\mathbf{k},\hat{\mathbf{p}}}$. We start with a discussion of the valence band Hamiltonian matrix of the k -independent SOI (H_{SO}). From Table II, one finds that the three invariant components of H_{SO} belong to the IRs of Γ_2^+ , Γ_3^+ and Γ_4^+ , which couples the highest valence band Γ_{2v}^+ to remote bands belong to Γ_1^+ , Γ_4^+ and Γ_3^+ , respectively. Therefore, in a basis $\{\Gamma_3^+, \Gamma_4^+, \Gamma_1^+, \Gamma_{2v}^+\}$, the matrix form of H_{SO} can be written

$$H_{\text{SO}}^{\text{hole}} = \begin{pmatrix} & & & i\delta_{32}\sigma_z \\ & & & i\delta_{42}\sigma_x \\ & & & i\delta_{12}\sigma_y \\ -i\delta_{32}\sigma_z & -i\delta_{42}\sigma_x & -i\delta_{12}\sigma_y & \end{pmatrix}, \quad (24)$$

where

$$\delta_{l2} = \sum_{\Gamma_l^+} \frac{i\hbar}{4m_0^2 c^2} \langle \Gamma_l^+ | \frac{\partial V}{\partial x_m} \hat{p}_n - \frac{\partial V}{\partial x_n} \hat{p}_m | \Gamma_{2v}^+ \rangle, \quad (25)$$

which are real numbers taking into account all remote bands belonging to the IR Γ_l^+ . Here, $\{lmn\}$ is a cyclic permutation of $\{1,2,3\}$ and $\{x_1, x_2, x_3\}$ correspond to $\{x, y, z\}$. By expanding the Pauli matrices, $H_{\text{SO}}^{\text{hole}}$ in Eq. (24) is an 8×8 matrix, where each basis function is the direct product of a spin-independent wave function and a spinor ($|\uparrow\rangle$ or $|\downarrow\rangle$, eigenstates of σ_z). Note that the lack of matrix elements other than those involving Γ_{2v}^+ in Eq. (24) does not imply that they are zero; rather, we focus here only on the matrix elements that are important in determining the valence band eigenvectors to lowest order.

$H_{\text{SO},\mathbf{k}}$ in Eq. (6) gives a small correction to H_{SO} that is usually negligible, since $|\hbar\mathbf{k}|$ is comparable with $|\mathbf{p}|$ only when \mathbf{k} reaches the zone edge. In phosphorene, however, due to the unusually flat valence band, k_y of hole states can be relatively large ($\gtrsim 10\%$ of π/a_y), and the resulting $H_{\text{SO},\mathbf{k}}$ cannot be ignored. The components of $H_{\text{SO},\mathbf{k}}$ transform like polar vectors as shown in Table II and for simplicity we only keep the more important k_y -related terms. Applying the same procedure as above, we obtain

the matrix form of $H_{\text{SO},\mathbf{k}}$ for hole states as

$$H_{\text{SO},\mathbf{k}}^{\text{hole}} = \begin{pmatrix} & i\alpha_{42}k_y\sigma_z & -i\alpha_{32}k_y\sigma_x \\ -i\alpha_{42}k_y\sigma_z & & \\ i\alpha_{32}k_y\sigma_x & & \end{pmatrix}, \quad (26)$$

which is a 6×6 matrix in the basis $\{\Gamma_{2v}^+, \Gamma_4^-, \Gamma_3^-\} \otimes \{\uparrow, \downarrow\}$. Again, we are only interested in the matrix elements that couple to Γ_{2v}^+ in lowest order. The α parameters in Eq. (26) are

$$\alpha_{32} = \sum_{\Gamma_3^-} \frac{i\hbar^2}{4m_0^2c^2} \langle \Gamma_3^- | \frac{\partial V}{\partial z} | \Gamma_{2v}^+ \rangle, \quad \text{and} \quad (27)$$

$$\alpha_{42} = \sum_{\Gamma_4^-} \frac{i\hbar^2}{4m_0^2c^2} \langle \Gamma_4^- | \frac{\partial V}{\partial x} | \Gamma_{2v}^+ \rangle. \quad (28)$$

The essential spin-orbit interaction of hole states is now captured by $H_{\text{SO}}^{\text{hole}} \oplus H_{\text{SO},\mathbf{k}}^{\text{hole}}$, reducible to a 12×12 matrix because of the redundant Γ_{2v}^+ . In combination with the spin-independent H_0 and $H_{\mathbf{k},\hat{\mathbf{p}}}$ operators discussed in the previous section, one can diagonalize the total Hamiltonian and obtain the spin-dependent eigenstates for holes.

Several simplifying approximations can be made. Because it appears in the same matrix element and is much smaller than the $P_{x1}k_x$ terms in Eq. (7), $\alpha_{42}k_y\sigma_z$ in Eq. (26) can reasonably be ignored. In addition, the P_yk_y terms (coupling between Γ_{2v}^+ and Γ_1^- bands) can be neglected for two reasons: (i) the amplitudes of P_{y2} and P_{y4} are small; and (ii) the effect from Γ_1^- bands below and above Γ_{2v}^+ counteract each other near the Γ -point (reflected by the flat band there).

To avoid lengthy summations and energy denominators, we define the following quantities related to the δ , α and P parameters:

$$\Delta_{l2} = \sum_{\Gamma_l^+} \frac{i\hbar}{4m_0^2c^2} \frac{\langle \Gamma_l^+ | \frac{\partial V}{\partial x_m} \hat{p}_n - \frac{\partial V}{\partial x_n} \hat{p}_m | \Gamma_{2v}^+ \rangle}{E_{\Gamma_l^+} - E_{\Gamma_{2v}^+}}, \quad (29)$$

$$A_{32}k_y = \sum_{\Gamma_3^-} \frac{i\hbar^2}{4m_0^2c^2} \frac{\langle \Gamma_3^- | \frac{\partial V}{\partial z} | \Gamma_{2v}^+ \rangle k_y}{E_{\Gamma_3^-} - E_{\Gamma_{2v}^+}}, \quad \text{and} \quad (30)$$

$$\Pi_{x1}k_x = \frac{P_{x1}k_x}{E_g}. \quad (31)$$

Because of their origins in the $H_{\mathbf{k},\hat{\mathbf{p}}} \gg H_{\text{SO}} \gg H_{\text{SO},\mathbf{k}}$ perturbation terms, the hierarchy between these unitless parameters is $A_{32}k_y \ll \Delta_{l2} \ll \Pi_{x1}k_x \ll 1$.

Each spin-dependent eigenvector includes 12 coefficients corresponding to the 12 basis functions which span the subspace of six IRs $\{\Gamma_3^+, \Gamma_4^+, \Gamma_1^+, \Gamma_{2v}^+, \Gamma_{4c}^-, \Gamma_3^-\}$ and the two spinors. We write the spin-dependent eigenvectors in the form of Eqs. (22) and (23) giving 2×6 matrices:

$$|h\uparrow_{\perp}\rangle = \begin{pmatrix} i\Delta_{32} & 0 & 0 & 1 & \Pi_{x1}k_x & 0 \\ 0 & i\Delta_{42} & \Delta_{12} & 0 & 0 & -iA_{32}k_y \end{pmatrix}, \quad \text{and} \quad (32)$$

$$|h\downarrow_{\perp}\rangle = \begin{pmatrix} 0 & i\Delta_{42} & -\Delta_{12} & 0 & 0 & -iA_{32}k_y \\ -i\Delta_{32} & 0 & 0 & 1 & \Pi_{x1}k_x & 0 \end{pmatrix}. \quad (33)$$

Here ‘h’ stands for ‘hole’ and the subscript ‘ \perp ’ indicates that the spin orientation z is out of plane. Notice that, before the trivial normalization, the dominant coefficients have the value of 1, corresponding to the $|\Gamma_{2v}^+\uparrow\rangle$ ($|\Gamma_{2v}^+\downarrow\rangle$) basis function in $|h\uparrow_{\perp}\rangle$ ($|h\downarrow_{\perp}\rangle$).

Eqs. (32) and (33) explicitly indicate the spin-purity of the eigenstates. One can evaluate the total square amplitude of the minority-spin components (the so-called ‘spin mixing’ coefficient), which is approximately $\Delta_{42}^2 + \Delta_{12}^2$ (the $A_{42}^2k_y^2$ term is a small correction). In Eq. (29), the energy denominators are several eV or more, while the remainder are within the same order of the δ_{l2} parameters in Eq. (25). It is known that the dominant contribution to spin-orbit coupling is from the part of wavefunctions orthogonal to the core states, which are populated in the vicinity of the nucleus where the atomic potential changes drastically.^{44,45} As in Si, these core electrons are $2p$ states, so we can estimate using the same parameters: $\delta_{l2} \sim \text{meV}$.³⁸ This value then gives $\Delta_{l2} \sim 10^{-3}$, so the spin mixing coefficient for holes in phosphorene should be similar to that of conduction band electrons in Si, which is approximately $10^{-5} - 10^{-6}$.

Eqs. (32) and (33) are fundamental in helping us understand the spin-flip process, in which a transition occurs between $|h\uparrow_{\perp}\rangle$ and $|h\downarrow_{\perp}\rangle$ during momentum scattering. As an example, we analyze the symmetry of the Elliott-Yafet (EY) spin-flipping process due to scattering by small- k long-wavelength acoustic phonons (in-phase quasi-uniform vibration of atoms). This is the dominant spin relaxation mechanism that limits the intrinsic spin-lifetime in such a centrosymmetric system at finite temperature.

The Elliott term⁴² proportional to ∇V has the same symmetry of a polar vector or the p orbitals of Γ_2^- in Fig. 2, Γ_3^- in Fig. 3(a) and Γ_4^- in Fig. 3(b). It couples the same spin components between $|h\uparrow_{\perp}\rangle$ and $|h\downarrow_{\perp}\rangle$. Eqs. (32) and (33) show that this happens between Γ_{2v}^+ and Γ_3^- (with the coefficients 1 and $-A_{32}k_y$), as well as between Γ_{4c}^- and Γ_1^+ (with the coefficients $\Pi_{x1}k_x$ and Δ_{12}), and the responsible phonon mode is the Γ_4^- -related $\frac{\partial V}{\partial z}$ Elliott term (out-of-plane motion of atoms, or flexural phonons).

On the other hand, the Yafet operator that couples opposite spin components⁴³ between $|h\uparrow_{\perp}\rangle$ and $|h\downarrow_{\perp}\rangle$ is proportional to ∇H_{SO} , which is the gradient of an axial vector with symmetry

$$\begin{aligned} & (\Gamma_4^- \oplus \Gamma_3^- \oplus \Gamma_2^-) \otimes (\Gamma_4^+ \oplus \Gamma_3^+ \oplus \Gamma_2^+) \\ & = 3\Gamma_1^- \oplus 2\Gamma_2^- \oplus 2\Gamma_3^- \oplus 2\Gamma_4^-. \end{aligned} \quad (34)$$

Examining Eqs. (32) and (33), one sees that the dominant coupling is between Γ_{2v}^+ and Γ_{4c}^- by one of the two Γ_3^- IRs in Eq. (34) that is related to $\frac{\partial}{\partial z} \left(\frac{\partial V}{\partial z} p_x - \frac{\partial V}{\partial x} p_z \right) \sigma_y$. This term also corresponds to flexural phonons [the other term belonging to Γ_3^- IR is $\frac{\partial}{\partial y} \left(\frac{\partial V}{\partial x} p_y - \frac{\partial V}{\partial y} p_x \right) \sigma_z$, which does not flip the spin].

The same formalism can be applied to study the spin-dependent conduction band electrons. Here, we list the

expressions for Hamiltonian matrices and spin-dependent eigenstates of the lowest eigenvalue (conduction band minimum). In a basis $\{\Gamma_3^-, \Gamma_2^-, \Gamma_1^-, \Gamma_{4c}^-\}$, H_{SO} for Γ_{4c}^- electrons is

$$H_{\text{SO}}^{\text{electron}} = \left(\begin{array}{c|c} & \begin{array}{l} i\delta_{34}\sigma_y \\ i\delta_{24}\sigma_x \\ i\delta_{14}\sigma_z \end{array} \\ \hline \begin{array}{l} -i\delta_{34}\sigma_y \\ -i\delta_{24}\sigma_x \\ -i\delta_{14}\sigma_z \end{array} & \end{array} \right), \quad (35)$$

where

$$\delta_{l4} = \sum_{\Gamma_l^-} \frac{\hbar^2}{4m_0^2c^2} \langle \Gamma_l^- | \frac{\partial V}{\partial x_m} \hat{p}_n - \frac{\partial V}{\partial x_n} \hat{p}_m | \Gamma_{4c}^- \rangle. \quad (36)$$

As in Eq. (26) for holes, the $H_{\text{SO},\mathbf{k}}$ matrix for electrons in the k_y direction, using the basis $\{\Gamma_{4c}^-, \Gamma_2^+, \Gamma_1^+\}$, reads

$$H_{\text{SO},\mathbf{k}}^{\text{electron}} = \left(\begin{array}{c|c} & \begin{array}{l} i\alpha_{24}k_y\sigma_z \\ -i\alpha_{14}k_y\sigma_x \end{array} \\ \hline \begin{array}{l} -i\alpha_{24}k_y\sigma_z \\ i\alpha_{14}k_y\sigma_x \end{array} & \end{array} \right), \quad (37)$$

where the α parameters are

$$\alpha_{24} = \sum_{\Gamma_2^+} \frac{i\hbar^2}{4m_0^2c^2} \langle \Gamma_2^+ | \frac{\partial V}{\partial z} | \Gamma_{4c}^- \rangle, \quad \text{and} \quad (38)$$

$$\alpha_{14} = \sum_{\Gamma_1^+} \frac{i\hbar^2}{4m_0^2c^2} \langle \Gamma_1^+ | \frac{\partial V}{\partial x} | \Gamma_{4c}^- \rangle. \quad (39)$$

As in Eqs. (29) and (30), we define

$$\Delta_{l4} = \sum_{\Gamma_l^-} \frac{i\hbar}{4m_0^2c^2} \frac{\langle \Gamma_l^+ | \frac{\partial V}{\partial x_m} \hat{p}_n - \frac{\partial V}{\partial x_n} \hat{p}_m | \Gamma_{4c}^- \rangle}{E_{\Gamma_l^-} - E_{\Gamma_{4c}^-}}, \quad \text{and} \quad (40)$$

$$A_{14}k_y = \sum_{\Gamma_1^+} \frac{i\hbar^2}{4m_0^2c^2} \frac{\langle \Gamma_1^+ | \frac{\partial V}{\partial z} | \Gamma_{4c}^- \rangle k_y}{E_{\Gamma_1^+} - E_{\Gamma_{4c}^-}}. \quad (41)$$

The resulting spin-dependent electron eigenstates in the basis $\{\Gamma_3^-, \Gamma_2^-, \Gamma_1^-, \Gamma_{4c}^-, \Gamma_{2v}^+, \Gamma_1^+\}$ are

$$|e \uparrow_{\perp}\rangle = \begin{pmatrix} 0 & 0 & i\Delta_{14} & 1 & \Pi_{x1}k_x & 0 \\ \Delta_{34} & i\Delta_{24} & 0 & 0 & 0 & -iA_{14}k_y \end{pmatrix}, \quad \text{and} \quad (42)$$

$$|e \downarrow_{\perp}\rangle = \begin{pmatrix} -\Delta_{34} & i\Delta_{24} & 0 & 0 & 0 & -iA_{14}k_y \\ 0 & 0 & -i\Delta_{14} & 1 & \Pi_{x1}k_x & 0 \end{pmatrix}. \quad (43)$$

B. Anisotropy of spin-dependent properties

We naturally expect that the orthorhombic inequivalence of the three orthogonal armchair, zigzag, and out-of-plane axes will induce anisotropy of the spin-dependent properties of electrons and holes. Already from our analysis of the band dispersion, we can see an obvious anisotropy in the spin-diffusion length $\lambda_s =$

$\sqrt{\tau_s D}$, where the carrier diffusion coefficient D is related to the anisotropic effective mass. However, there is an additional contribution: the spin lifetime τ_s also has an anisotropy, related in this case not to the wavevector direction, but rather to the spin orientation.

In the previous subsection, we have derived the spin-dependent Hamiltonian and eigenstates with the spin orientation in the out-of-plane z -direction. However, in most spin-injection experiments, the spin orientation is fixed by the magnetization of ferromagnetic thin-film contacts with an in-plane easy axis. It is therefore more relevant to study the spin-dependent eigenstates and related properties with the spin quantization axis z in-plane. Of course, the spatial symmetry of the system is invariant regardless of the coordinate system we choose, and so are the properties of IRs and the relations between them (Table III); only the coordinate labels change.

First, we calculate the spin-dependent properties of hole states under a new coordinate system where z is chosen to be along the armchair, x along the zigzag and y along the out-of-plane direction. We apply the cyclic permutation $xyz \rightarrow zxy$ to the coordinates in Fig. 1(a), and the corresponding invariant components in Table II (note that one could also keep the coordinate system unchanged but alternatively derive spin-dependent eigenstates from linear combination of $|\hbar \uparrow_{\perp}\rangle$ and $|\hbar \downarrow_{\perp}\rangle$, and $|e \uparrow_{\perp}\rangle$ and $|e \downarrow_{\perp}\rangle$, according to the chosen spin orientation). The spin-dependent Hamiltonian can be derived straightforwardly, so we do not repeat the previous procedures but rather give the result of the spin-dependent eigenstates.

Like Eqs. (32) and (33), the spin-dependent eigenvectors for valence-band holes under the new coordinate system also includes 12 coefficients corresponding to the 12 basis functions which expand the subspace of six IRs $\{\Gamma_3^+, \Gamma_4^+, \Gamma_1^+, \Gamma_{2v}^+, \Gamma_{4c}^-, \Gamma_3^-\}$ and the two spinors. In the form of Eqs. (22) and (23), they read

$$|\hbar \uparrow_{\text{ac}}\rangle = \begin{pmatrix} 0 & i\Delta_{42} & 0 & 1 & \Pi_{z1}k_z & -iA_{32}k_x \\ \Delta_{32} & 0 & i\Delta_{12} & 0 & A_{42}k_x & 0 \end{pmatrix}, \quad \text{and} \quad (44)$$

$$|\hbar \downarrow_{\text{ac}}\rangle = \begin{pmatrix} -\Delta_{32} & 0 & i\Delta_{12} & 0 & -A_{42}k_x & 0 \\ 0 & -i\Delta_{42} & 0 & 1 & \Pi_{z1}k_z & iA_{32}k_x \end{pmatrix}. \quad (45)$$

Here, the subscript ‘ac’ stands for ‘armchair’ and indicates the spin orientation. Π_{z1} has the same value as Π_{x1} defined by Eq. (31) since we have only changed the labeling from x to z . Also, similar to the definition of A_{32} in Eq. (30), we have

$$A_{42}k_y = \sum_{\Gamma_4^-} \frac{i\hbar^2}{4m_0^2c^2} \frac{\langle \Gamma_4^- | \frac{\partial V}{\partial z} | \Gamma_{2v}^+ \rangle k_y}{E_{\Gamma_4^-} - E_{\Gamma_{2v}^+}}. \quad (46)$$

Eqs. (44) and (45) directly show that spin-mixing to lowest order is $\Delta_{32}^2 + \Delta_{12}^2$, different from the previous case ($\Delta_{42}^2 + \Delta_{12}^2$) when the spin orientation z is out-of-plane. It will be shown that if z is along the zigzag direction, the spin mixing is $\Delta_{32}^2 + \Delta_{42}^2$ [see Eqs. (47) and (48)]. The

anisotropy of the spin-mixing is generally reflected in the definition of Eq. (29) by the energy denominators, while the numerators scale similarly, due to their major origins related to the $2p$ core states, as previously discussed.^{44,45} Numerical calculation shows that, for the Γ_{2v}^+ hole band, the closest Γ_3^+ is the fourth conduction band approximately 3.5 eV above, while the closest neighboring Γ_4^+ and Γ_1^+ bands are the second and third valence bands (not shown in Fig. 5) that are approximately 1.8 eV below. We therefore estimate that the spin mixing with z in-plane is approximately half of that with z out-of-plane, and the Elliott-process-limited spin lifetime is consequently ~ 4 times longer.

A more intriguing feature of the anisotropy is that of the phonon polarization in spin-flip scattering. Again, we take the interaction with long wavelength acoustic phonons as an example. In contrast to the case when z is out-of-plane, here the coupling of the dominant Γ_{2v}^+ band by the Elliott operator to Γ_3^- vanishes, since the coefficient for $\Gamma_3^-\uparrow(\downarrow)$ in $|h\downarrow_{ac}(\uparrow_{ac})\rangle$ is zero. However, the coupling between Γ_{2v}^+ and Γ_4^- survives, with the coefficient $-A_{42}k_y$. More importantly, the interaction belongs to $\Gamma_3^- = \Gamma_{2v}^+ \otimes \Gamma_4^-$, which still corresponds to $\frac{\partial V}{\partial z}$, but is now related to in-plane, instead of flexural, phonons.

It is well-known that, due to their quadratic dispersion relation, the thermal population of flexural phonons in 2D materials diverges when the phonon wavevector \mathbf{q} approaches zero. Such a singularity does not exist in the case of in-plane phonons with linear dispersion. The intrinsic spin lifetime in 2D materials is thus essentially limited by the interaction with flexural phonons while the influence from in-plane phonons is much less crucial.⁴ However, here in phosphorene, for spins oriented in the armchair direction the Elliott spin-flip coupling of the dominant Γ_{2v}^+ component via flexural phonons is excluded by symmetry.

We have seen that scattering by acoustic phonons ultimately determines the upper bound of the spin lifetime in phosphorene. However, this intrinsic mechanism will be superseded by various extrinsic spin relaxation mechanisms in anything other than the most pure, well-isolated samples. Carrier spins in 2D materials are especially sensitive to extrinsic effects such as interactions with substrate and contacts, scattering with impurities or defects, and the influence of deformation such as nanoripples and strain. As long as these spin-flip processes are within the perturbative regime, the spin-dependent eigenvectors can be effectively used to determine whether a certain process is symmetry-allowed, as well as its orientation dependence. The strength of the interaction can be evaluated by the coefficients in these eigenvectors, calculated with the assistance of numerical schemes able to yield the coupling amplitude between basis functions.

Before closing this section, we derive expressions for the spin-dependent hole eigenvectors for the remaining orientation with z along the zigzag direction by applying the permutation $xyz \rightarrow yzx$ to the table of invariants. Using a basis $\{\Gamma_3^+, \Gamma_4^+, \Gamma_1^+, \Gamma_{2v}^+, \Gamma_{4c}^-, \Gamma_3^-\}$, the eigenvec-

tors read

$$|h\uparrow_{zz}\rangle = \begin{pmatrix} 0 & 0 & i\Delta_{12} & 1 & \Pi_{y1}k_y & 0 \\ i\Delta_{32} & \Delta_{42} & 0 & 0 & iA_{42}k_z & -A_{32}k_z \end{pmatrix}, \text{ and} \quad (47)$$

$$|h\downarrow_{zz}\rangle = \begin{pmatrix} i\Delta_{32} & -\Delta_{42} & 0 & 0 & iA_{42}k_z & A_{32}k_z \\ 0 & 0 & -i\Delta_{12} & 1 & \Pi_{y1}k_y & 0 \end{pmatrix}. \quad (48)$$

The subscript ‘zz’ stands for ‘zigzag’. Also, we give the spin-dependent eigenvectors of the conduction-band electron states for the spin orientation aligned with both in-plane axes, in a basis $\{\Gamma_3^-, \Gamma_2^-, \Gamma_1^-, \Gamma_{4c}^-, \Gamma_{2v}^+, \Gamma_1^+\}$. For z along the armchair direction, the eigenvectors are

$$|e\uparrow_{ac}\rangle = \begin{pmatrix} 0 & i\Delta_{24} & 0 & 1 & \Pi_{z1}k_z & -iA_{14}k_x \\ i\Delta_{34} & 0 & \Delta_{14} & 0 & -A_{24}k_x & 0 \end{pmatrix}, \text{ and} \quad (49)$$

$$|e\downarrow_{ac}\rangle = \begin{pmatrix} i\Delta_{34} & 0 & -\Delta_{14} & 0 & A_{24}k_x & 0 \\ 0 & -i\Delta_{24} & 0 & 1 & \Pi_{x1}k_x & iA_{14}k_y \end{pmatrix}. \quad (50)$$

For z along the zigzag direction, they are

$$|e\uparrow_{zz}\rangle = \begin{pmatrix} i\Delta_{34} & 0 & 0 & 1 & \Pi_{y1}k_y & 0 \\ 0 & \Delta_{24} & i\Delta_{14} & 0 & iA_{24}k_z & A_{14}k_z \end{pmatrix}, \text{ and} \quad (51)$$

$$|e\downarrow_{zz}\rangle = \begin{pmatrix} 0 & -\Delta_{24} & i\Delta_{14} & 0 & iA_{24}k_z & -A_{14}k_z \\ -i\Delta_{34} & 0 & 0 & 1 & \Pi_{y1}k_y & 0 \end{pmatrix}. \quad (52)$$

V. SUMMARY

We have detailed the myriad ways in which phosphorene’s structural in-plane asymmetry is manifest in the anisotropy of charge and spin properties of its electrons and holes, all of which are otherwise obscured by the many numerical methods previously applied to the problem. We have elucidated the origin of the band dispersion anisotropy near the gap edge, which is due to the specific directional preference of the coupling between conduction and valence bands and governs various transport and optical properties. By analyzing the symmetry of spin-orbit coupling, we have derived compact spin-dependent eigenstates of electrons and holes for all high-symmetry quantization axes. As an example of the utility of these eigenstates, we investigated the valence band anisotropy of the Elliott-Yafet spin-relaxation process. By incorporating the relevant invariant components into our model, such as those of external applied fields, mechanical strain, and quantum confinement, this theory is highly extensible to the analysis of many other relevant circumstances of interest.

Importantly, our theory provides guidance for experimental efforts to empirically confirm and quantify these charge and spin phenomena. Valence band properties like the effective mass anisotropy and possible indirect bandgap are most directly compared to results from ARPES.^{25,27} This ultra-high vacuum surface-sensitive

method is especially convenient since electrical contact to phosphorene transport layers has not yet been realized, in part due to environmental sensitivity and subsequent degradation.²⁰ Even without metallic electrodes, basic transport properties can be determined with e.g. microwave Hall mobility measurement.⁴⁶ However, investigation into many other properties (such as thermal and excitonic transport, weak localization or antilocalization, etc) may require fabrication of true electronic devices.

Optical non-contact techniques are also very useful in verifying the linear polarimetry in the visible spectrum, enabled by the dipole selection rules. However, with the expected inefficiency of optical orientation in this material, electrical techniques are required to measure anisotropy of the spin relaxation. Once single phosphorene layers can be stabilized for device processing and fabrication, four-terminal nonlocal geometry devices in the presence of oblique magnetic fields (to precess spins out-of-plane) will be especially applicable.⁴⁷

In closing, we are obliged to point out the presence of

secondary features of the conduction and valence bands that cannot be captured simply by the zone-center symmetries. For example, satellite valleys may play a role in transport properties of phosphorene when a high electric field accelerates and heats mobile charge carriers. Interestingly, secondary conduction band valleys are predicted by DFT calculation along the k_y direction, whereas the valence band valleys are along the k_x direction, several hundred meV from the band edge.

ACKNOWLEDGMENTS

We thank Dr. Yang Song for carefully reading the manuscript and providing valuable suggestions. We gratefully acknowledge support from the Office of Naval Research under contract N000141410317, the National Science Foundation under contract ECCS-1231855, and the Defense Threat Reduction Agency under contract HDTRA1-13-1-0013.

-
- * pengke@umd.edu
- ¹ B. Aufray, A. Kara, S. B. Vizzini, H. Oughaddou, C. LéAndri, B. Ealet, and G. Le Lay, *Appl. Phys. Lett.* **96**, 183102 (2010); B. Lalmi, H. Oughaddou, H. Enriquez, A. Kara, S. B. Vizzini, B. N. Ealet, and B. Aufray, *Appl. Phys. Lett.* **97**, 223109.
 - ² M. E. Dvila, L. Xian, S. Cahangirov, A. Rubio, and G. L. Lay, *New Journal of Physics* **16**, 095002 (2014).
 - ³ A. Barfuss, L. Dudy, M. R. Scholz, H. Roth, P. Höpfner, C. Blumenstein, *et al.*, *Phys. Rev. Lett.* **111**, 157205 (2013).
 - ⁴ Y. Song and H. Dery, *Phys. Rev. Lett.* **111**, 026601 (2013).
 - ⁵ M. Z. Hasan and C. L. Kane, *Rev. Mod. Phys.* **82**, 3045 (2010).
 - ⁶ N. Alem, R. Erni, C. Kisielowski, M. D. Rossell, W. Gannett, and A. Zettl, *Phys. Rev. B* **80**, 155425 (2009).
 - ⁷ A. Morita, *Appl. Phys. A* **39**, 227 (1986).
 - ⁸ P. W. Bridgman, *J. Am. Chem. Soc.* **36**, 1344 (1914).
 - ⁹ Y. Maruyama, S. Suzuki, K. Kobayashi, and S. Tanuma, *Physica B+C* **105**, 99 (1981).
 - ¹⁰ R. Hultgren, N. S. Gingrich, and B. E. Warren, *J. Chem. Phys.* **3**, 351 (1935).
 - ¹¹ A. Brown and S. Rundqvist, *Acta Cryst.* **19**, 684 (1965).
 - ¹² R. W. Keyes, *Phys. Rev.* **92**, 580 (1953).
 - ¹³ D. Warschauer, *J. Appl. Phys.* **34**, 1853 (1963).
 - ¹⁴ S. Narita, Y. Akahama, Y. Tsukiyama, K. Muro, S. Mori, S. Endo, M. Taniguchi, M. Seki, S. Suga, A. Mikuni, and H. Kanzaki, *Physica B+C* **117-118**, Part 1, 422 (1983).
 - ¹⁵ H. Asahina and A. Morita, *J. Phys. C* **17**, 1839 (1984).
 - ¹⁶ T. Low, A. S. Rodin, A. Carvalho, Y. Jiang, H. Wang, F. Xia, and A. H. Castro Neto, *Phys. Rev. B* **90**, 075434 (2014).
 - ¹⁷ H. Kawamura, I. Shirovani, and K. Tachikawa, *Solid State Comm.* **49**, 879 (1984).
 - ¹⁸ M. Baba, Y. Nakamura, Y. Takeda, K. Shibata, A. Morita, Y. Koike, and T. Fukase, *J. Phys.: Cond. Mat.* **4**, 1535 (1992).
 - ¹⁹ S. P. Koenig, R. A. Doganov, H. Schmidt, A. H. Castro Neto, and B. Özyilmaz, *Appl. Phys. Lett.* **104**, 103106 (2014).
 - ²⁰ H. Liu, A. T. Neal, Z. Zhu, Z. Luo, X. Xu, D. Tomnek, and P. D. Ye, *ACS Nano* **8**, 4033 (2014).
 - ²¹ Y. Takao and A. Morita, *Physica B+C* **105**, 93 (1981); Y. Takao, H. Asahina, and A. Morita, *J. Phys. Soc. Japan* **50**, 3362 (1981).
 - ²² A. N. Rudenko and M. I. Katsnelson, *Phys. Rev. B* **89**, 201408 (2014).
 - ²³ H. Asahina, K. Shindo, and A. Morita, *J. Phys. Soc. Japan* **51**, 1193 (1982).
 - ²⁴ Y. Du, C. Ouyang, S. Shi, and M. Lei, *J. Appl. Phys.* **107**, 093718 (2010).
 - ²⁵ F. Xia, H. Wang, and Y. Jia, *Nature Comm.* **5**, 4458 (2014).
 - ²⁶ J. Q. and Xianghua Kong and Zhi-Xin Hu and Feng Yang and W. Ji, *Nature Comm.* **5**, 4475 (2014).
 - ²⁷ L. Li, Y. Yu, G. J. Ye, Q. Ge, X. Ou, H. Wu, D. Feng, X. H. Chen, and Y. Zhang, *Nature Nano.* **9**, 372 (2014).
 - ²⁸ A. Rodin, A. Carvalho, and A. Castro Neto, *Phys. Rev. Lett.* **112**, 176801 (2014).
 - ²⁹ T. Takahashi, K. Shirovani, S. Suzuki, and T. Sagawa, *Solid State Communications* **45**, 945 (1983).
 - ³⁰ V. Tran, R. Soklaski, Y. Liang, and L. Yang, *Phys. Rev. B* **89**, 235319 (2014).
 - ³¹ M. Buscema, D. J. Groenendijk, S. I. Blanter, G. A. Steele, H. S. J. van der Zant, and A. Castellanos-Gomez, *Nano Lett.* **14**, 3347 (2014).
 - ³² G. L. Bir and G. E. Pikus, *Symmetry and Strain-Induced Effects in Semiconductors* (New York, Wiley, 1974).
 - ³³ C. Bradley and A. Cracknell, *The mathematical theory of symmetry in solids: representation theory for point groups and space groups* (Clarendon, 1972).
 - ³⁴ P. Giannozzi *et al.*, *J. Phys.: Cond. Mat.* **21**, 395502 (2009).
 - ³⁵ P. Löwdin, *J. Chem. Phys.* **19**, 1396 (1951).

- ³⁶ V. Tran and L. Yang, *Phys. Rev. B* **89**, 245407 (2014).
- ³⁷ B. Huang, D. Monsma, and I. Appelbaum, *Phys. Rev. Lett.* **99**, 177209 (2007).
- ³⁸ P. Li and H. Dery, *Phys. Rev. Lett.* **107**, 107203 (2011).
- ³⁹ J. L. Cheng, M. W. Wu, and J. Fabian, *Phys. Rev. Lett.* **104**, 016601 (2010).
- ⁴⁰ R. Jansen, *Nature Mat.* **11**, 400408 (2012).
- ⁴¹ M. Dyakonov and V. Perel, *Sov. Phys. Solid State* **13**, 3023 (1972).
- ⁴² R. Elliott, *Phys. Rev.* **96**, 266 (1954).
- ⁴³ Y. Yafet, in *Solid State Physics*, Vol. 14, edited by F. Seitz and D. Turnbull (Academic Press, New York, 1963) pp. 1 – 98.
- ⁴⁴ L. Liu, *Phys. Rev.* **126**, 1317 (1962).
- ⁴⁵ G. Weisz, *Phys. Rev.* **149**, 504 (1966).
- ⁴⁶ A. M. Portis and D. Teaney, *J. Appl. Phys.* **29**, 1692 (1958).
- ⁴⁷ W. Han, K. Pi, K. M. McCreary, Y. Li, J. J. I. Wong, A. G. Swartz, and R. K. Kawakami, *Phys. Rev. Lett.* **105**, 167202 (2010).